

Are the double Fermi arcs of Dirac semimetals topologically protected?

Mehdi Kargarian, Mohit Randeria, and Yuan-Ming Lu

Department of Physics, The Ohio State University, Columbus, OH 43212, USA

(Dated: August 5, 2022)

Motivated by recent experiments on double Fermi arcs on the surface of Dirac semimetals (DSMs) Na₃Bi and Cd₃As₂, we raise the question posed in the title. We find that, in marked contrast to Weyl semimetals, the Fermi arcs of DSMs are not topologically protected in general, except at certain time-reversal invariant momenta. For a simple 4-band model with a pair of Dirac nodes at $\mathbf{k} = (0, 0, \pm Q)$ gapless surface states are protected only at $k_z = 0$. We identify symmetry allowed bulk perturbations that destroy Fermi arcs, but show that they are necessarily “small”, i.e., higher order than terms kept in usual $\mathbf{k} \cdot \mathbf{p}$ theory. We validate our conclusions about the absence of a topological invariant protecting the surface states in DSMs using a K-theory analysis for the space groups of Na₃Bi and Cd₃As₂.

PACS numbers: 73.43.-f, 73.20.-r, 73.43.Cd, 71.20.-b

CONTENTS

I. Introduction	1
II. Surface states in a minimal model of Dirac semimetals	2
A. 4-band minimal model and its symmetries	2
B. Simple arguments on why surface Fermi arcs are unstable	2
C. Numerical results	4
III. Topological classification of surface states in Cd ₃ As ₂ and Na ₃ Bi	4
A. Symmetry classification of Na ₃ Bi	4
1. Side surface (100)	5
2. Side surface (110)	6
3. Surface states at $k_z = 0, \pi$	7
B. Symmetry classification of Cd ₃ As ₂	7
1. Side surface (100)	8
2. Side surface (110)	8
IV. Conclusions	8
Acknowledgments	9
A. Equivalence between 4-band model (1) and effective $k \cdot p$ Hamiltonian for Cd ₃ As ₂ and Na ₃ Bi	9
B. 4-band Tight-binding Model for Dirac semimetal Na ₃ Bi	9
References	10

I. INTRODUCTION

In the last decade, condensed matter physics witnessed a large class of novel electronic materials characterized by their topological properties, such as quantized bulk response functions and robust surface states. Experimental discovery of topological insulators protected by

time reversal symmetry¹⁻³ greatly advanced our understanding of quantum states with nontrivial topology, which are beyond the description of symmetry breaking and local order parameters in the traditional Landau paradigm. Moreover, these topological properties also apply to metallic systems, where the gapless bulk band structures are featured by protected point or line nodes⁴⁻⁹. For the former case, the conduction and valence bands intersect at isolated points at the Fermi level, giving rise to low energy electron behaviors described by relativistic Dirac equations¹⁰. One outstanding example is the three-dimensional (3D) Dirac material, a 3D analogue of graphene, with nodal points at the Fermi level where the band dispersion is linear in all directions¹¹⁻¹³. The angle-resolved photoemission spectroscopy (ARPES) clearly observed the presence of linearly-dispersing energy bands near 3D Dirac nodes in the bulk of Na₃Bi^{14,15} and Cd₃As₂¹⁶⁻¹⁸. The observation of Fermi arcs¹⁹ in Na₃Bi and their peculiar quantum oscillations²⁰ have also been reported in Cd₃As₂.

In the presence of both time-reversal and inversion symmetries each Dirac node is described by a four-component Dirac fermion, which can be viewed as two degenerate Weyl fermions with opposite chirality. In Dirac semimetals, it is crystal symmetries that forbid these two opposite-chirality Weyl fermions to hybridize and open up a gap at each Dirac point^{11,21}. If separated in momentum-space, bulk Weyl nodes generally lead to open Fermi arcs on surfaces of system⁶ connecting two Weyl nodes with opposite chirality, as observed in non-centrosymmetric TaAs²²⁻²⁵. Therefore, when a pair of time-reversal-related Dirac nodes are located off the time reversal invariant momenta in the Dirac semimetal, a pair of Fermi arcs (“double Fermi arcs”) are expected to appear on certain surfaces of the system^{12,13} as shown schematically in Fig. 1(a). As pointed out in Ref. [26], the surface double Fermi arcs are stable perturbatively against a weak symmetry-breaking surface potential, although a strong surface potential can destroy them. A natural and important question is: are these “double Fermi arcs” in Dirac semimetals topologically

protected, similar to open Fermi arcs in Weyl semimetals? Unlike Weyl semimetals which need no extra symmetry protection^{6,27}, bulk-boundary correspondence in topological phases⁹ provide no obvious answer for Dirac semimetals, since the stability of bulk Dirac nodes require crystal rotation symmetries^{12,13} which are explicitly broken on open surfaces.

In this work we provide a negative answer to this question, by showing that the *surface double Fermi arcs can be continuously deformed into a closed pocket enclosing the surface zone center and to even a single point in Dirac semimetals without any symmetry breaking or bulk phase transition*, as illustrated in Fig. 1(b)-(c). We use K-theory^{5,28-31} to classify the topological stability of surface states in Dirac semimetals in the presence of time reversal, charge conservation and all space group symmetries in Dirac semimetals Cd₃As₂ and Na₃Bi. This classification indicates that topological protection for gapless surface states on side surfaces (parallel to \hat{z} -axis) of Dirac semimetals only exists in high-symmetry plane $k_z = 0$. This conclusion is supported by numerical calculations of surface spectral density in a minimal 4-band model^{12,13} for Dirac semimetal materials. As shown in Fig. 2, *the surface double Fermi arcs can be continuously deformed into a closed Fermi surface, or even a single surface Dirac node similar to topological insulator surfaces by adding symmetric perturbations*.

This paper is organized as follows. In section II we introduce the minimal 4-band model^{12,13,32} as simplest mode with two Dirac nodes in the bulk located off the center of Brillouin zone (BZ). Following simple arguments for why the double Fermi arcs on sides surfaces are unstable to symmetric perturbations, we show numerical results of surface and bulk spectral functions in the minimal 4-band model to support our conclusions. In section III we further use K-theory to classify the stability of surface states in Cd₃As₂ and Na₃Bi, to prove the validity of our conclusions beyond minimal 4-band model.

II. SURFACE STATES IN A MINIMAL MODEL OF DIRAC SEMIMETALS

In this section we restrict ourselves to a representative Dirac semimetal: a minimal 4-band model with $n = 4$ -fold rotational symmetry along \hat{z} -axis. Despite being simple, this model can capture the band inversion near the Γ point of BZ of Cd₃As₂. A simple model can also be adopted for the case of Na₃Bi with $n = 6$, which will be briefly discussed in Appendix B.

A. 4-band minimal model and its symmetries

The minimal 4-band model describing Dirac semimetal Cd₃As₂ is given as follows:

$$H_4(\mathbf{k}) = \varepsilon_{\mathbf{k}} + \left[t(\cos k_x + \cos k_y - 2) + t_z(\cos k_z - b) \right] \tau_z + \lambda \sin k_x \sigma_x \tau_x + \lambda \sin k_y \sigma_y \tau_x, \quad (1)$$

where $\vec{\sigma}$ and $\vec{\tau}$ are Pauli matrices for spin and orbital indices. $t(t_z)$ is in-plane (out of plane) hopping term and λ represents spin-orbit coupling (SOC) and we choose $b = \cos Q$. The dispersive term $\varepsilon_{\mathbf{k}}$ should be consistent with all symmetries of the system as follows and to be vanished at the nodes. Therefore, their roles are unimportant in examining the stability of Fermi arcs. We return to this point in Sec. II C.

As shown in Appendix A, in the long-wavelength limit this model³² is equivalent to the well-known effective $k \cdot p$ Hamiltonian around Γ point for Dirac semimetal materials^{12,13}, up to a unitary transformation in the fermion basis. The spectrum is gapped over entire Brillouin zone except at two discrete points $k_z = \pm Q$, where the low energy spectrum is described by linearly-dispersing Dirac fermions. It is immediate to see that the Hamiltonian has time-reversal $\Theta = i\sigma_y \cdot \mathcal{K}$, inversion I , two-fold rotation $C_{2,x(y)}$ and n -fold rotation $C_{n,z}$ ($n = 4$ for Cd₃As₂ and $n = 6$ for Na₃Bi) symmetries as follows.

$$\Theta^{-1} H(\mathbf{k}) \Theta = H(-\mathbf{k}), \quad U_I^{-1} H(\mathbf{k}) U_I = H(-\mathbf{k}), \quad (2)$$

$$U_{C_{2,x}}^{-1} H(k_x, k_y, k_z) U_{C_{2,x}} = H(k_x, -k_y, -k_z), \quad (3)$$

$$U_{C_{2,y}}^{-1} H(k_x, k_y, k_z) U_{C_{2,y}} = H(-k_x, k_y, -k_z), \quad (4)$$

$$U_{C_{n,z}}^{-1} H(k_{\pm}, k_z) U_{C_{n,z}} = H(e^{\pm i \frac{2\pi}{n}} k_{\pm}, k_z), \quad (5)$$

where $k_{\pm} = k_x \pm ik_y$. The operators U 's describe the matrix representations of symmetry operation in spin and orbital basis. As written the Hamiltonian in (1) in this form, the symmetry operators should be as follows: inversion $U_I = \tau_z$, two-fold rotation $U_{C_{2,x(y)}} = i\sigma_{x(y)}$ and n -fold rotation $U_{C_{n,z}} = e^{i\pi\sigma_z(1-2\tau_z)/n}$. Note that this model also has mirror reflection symmetries with respect to major planes:

$$U_{R_i} = U_{C_{2,i}} U_I = i\sigma_i \tau_z : \quad k_i \rightarrow -k_i. \quad (6)$$

where $i = x, y, z$.

B. Simple arguments on why surface Fermi arcs are unstable

In this subsection we show that the surface Fermi arcs of side surfaces of minimal model above are not topologically protected by (i) examining the instability of one-dimensional counter-propagating edge states of 2D slices of BZ, (ii) proving the existence of extra mass term in the gapped Dirac Hamiltonian of a two-dimensional plane with any fixed $k_z \notin \{\pm Q, 0, \pi\}$, and (iii) adding symmetric terms to the full 3D Hamiltonian. We further argue

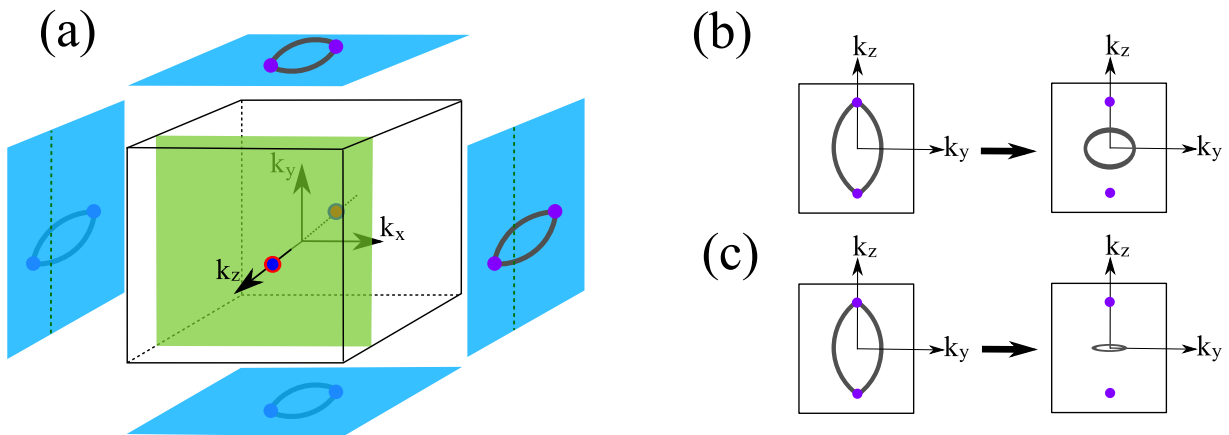


FIG. 1. (Color online) (a) Schematic \mathbf{k} -space picture showing the location of Dirac nodes each superimposed of two Weyl nodes (red and blue) along k_z axis in bulk Brillouin zone (BZ) and the possible double Fermi arcs on the surface BZ's, shown as blue squares. Note that surfaces perpendicular to z axis have no arcs. A 2D slice of BZ perpendicular to k_z axis is shown as green square projected to green dashed lines on side surfaces, where we only showed for (100) side surface. (b, c) Continuous deformation of double Fermi arcs on (100) side surface by coupling zero modes on Fermi arcs shown as dashed double arrows. Perturbations near the projected node as shown in left surface BZ in (b) can deform the Fermi arcs to a closed contour in right surface BZ in (b). Most parts of latter can be gapped out by coupling more states on double Fermi arcs as shown in left surface BZ in (c), which leaves behind only gapless helical modes concentrated around the center of surface BZ in (c).

that projection of bulk nodes onto surface still remain the gapless as additional terms don't gap the nodes. Moreover, the 2D slices located at $k_z = 0, \pi$ can still support the gapless edge states as they have extra symmetry.

Side surfaces parallel to \hat{z} axis are expected to support surface states as shown schematically in Fig. 1(a) (see also numerical results in Fig. 2 (a-f) for contrast). We show that surface states in any two-dimensional plane with fixed $k_z \notin \{\pm Q, 0, \pi\}$ shown as green square in Fig. 1(a), are unstable against symmetry-preserving perturbations and can be destroyed without breaking symmetry. In the following we'll first present simple arguments for this statement. Our arguments are supported by numerical studies of the minimal 4-band model (1), and by symmetry classification based on K-theory for material with any number of bands and richer symmetry in the following section.

Without loss of generality, let us consider open side surface (100) for an illustration. This side surface only preserves the following symmetries: time reversal Θ , mirror reflections R_y, R_z and their combinations. Therefore a generic fixed- k_z plane at $k_z \neq 0, \pi$ with open (100) surface only respects two symmetry operations: mirror reflection $U_{R_y} = \nu \sigma_y \tau_z$ w.r.t. \hat{y} -plane, and the combination $\Theta_{R_z} = \Theta U_{R_z} = \nu \sigma_x \tau_z \cdot \mathcal{K}$ of time reversal and mirror w.r.t. \hat{z} -plane

$$\Theta_{R_z}^{-1} \tilde{H}(k_x, k_y) \Theta_{R_z} = \tilde{H}(-k_x, -k_y), \quad (7)$$

$$U_{R_y}^{-1} \tilde{H}(k_x, k_y) U_{R_y} = \tilde{H}(k_x, -k_y). \quad (8)$$

Note that $\Theta_{R_z}^2 = 1$. Note that the usual time reversal operation squares as $\Theta^2 = -1$ for spin- $\frac{1}{2}$ fermions in the presence of SOC.

(i) First suppose there is a pair of counter-propagating gapless edge states in fixed- k_z plane on (100) surface, described by $H_{edge} = \hbar v_F \sum_{k_y} k_y \psi_{k_y}^\dagger \mu_z \psi_{k_y}$ where $\psi_{k_y}^T = (\psi_{R, k_y}, \psi_{L, k_y})$ is a two-component spinor of right and left movers. We are using Pauli matrix μ_z to label edge states which are spin-orbital and momentum coupled. Note that here we are making $\varepsilon_{\mathbf{k}} = 0$ leading the edge states to cross at $k_y = 0$. The more general case will be discussed in Sec. II C. Generically the two symmetry operations on the edge states are represented by $\Theta_{R_z} = \nu \mu_x \cdot \mathcal{K}$ and $U_{R_y} = \nu \mu_y$. Clearly the gapless edge states can be destroyed by adding a symmetry-preserving perturbation $\hat{M} = m \sum_{k_y} \psi_{k_y}^\dagger \mu_y \psi_{k_y}$, since $[\Theta_{R_z}, \mu_y] = [U_{R_y}, \mu_y] = 0$.

(ii) The instability of surface states in a generic fixed- k_z plane can also be understood within classification scheme²⁸⁻³⁰ of topological insulators, which will be elaborated and applied to real materials in the next section. Consider a 2D Dirac Hamiltonian of gapped insulator at fixed- $k_z \neq \pm Q$ as follows

$$\tilde{H}_D = k_x \gamma_x + k_y \gamma_y + m \gamma_0, \quad (9)$$

where $\gamma_x = \sigma_x \tau_x$, $\gamma_y = \sigma_y \tau_x$ and $\gamma_0 = \tau_z$ are Dirac matrices in the minimal model. The associated topological classification is trivial if an extra mass term $m' \gamma'_0$ preserving symmetries and anti-commuting with all Dirac matrices $\gamma_{x,y,0}$ can be added to the Hamiltonian above, since the topological phase ($m > 0$) can be continuously tuned into a trivial phase ($m < 0$) without gap closing at $m = 0$. Such a term indeed exists as $\gamma'_0 = \sigma_z \tau_x$, symmetric under operations Θ_{R_z} and U_{R_y} . Therefore side surface states within a generic $k_z \neq 0, \pi$ plane are not topologically protected.

In contrast, the planes located at $k_z = 0, \pi$ have higher symmetry including time reversal Θ . Since $\Theta^2 = -1$ for spin- $\frac{1}{2}$ electrons, time-reversal-invariant (TRI) $k_z = 0, \pi$ planes as a two-dimensional system can support a Z_2 topological index associated with quantum spin Hall (QSH) effect³³⁻³⁶. Meanwhile in Dirac semimetal materials Cd_3As_2 and Na_3Bi , there is a nonsymmorphic glide reflection g_c containing half translation along \hat{z} -axis, which serves as a mirror reflection for $k_z = 0, \pi$ planes satisfying $(g_c)^2 = -1(+1)$ for $k_z = 0(\pi)$. Generically such nonsymmorphic glide reflections guarantees that the Z_2 index must be trivial in $k_z = \pi$ plane³⁷, which will be elaborated in next section. Therefore in these materials, only $k_z = 0$ plane can support a nontrivial Z_2 index. A simple calculation of Z_2 index³⁸ shows that $k_z = 0$ plane is indeed a nontrivial QSH insulator. As a result, there are robust gapless surface states on side surfaces at least near $k_z = 0$ plane.

(iii) We can even go beyond the 1D edges and 2D slices and find additional terms preserving all symmetries of 3D system. In the 4-band minimal model (1), such a symmetric perturbation is simply $\delta H_4(\mathbf{k}) = f(\mathbf{k})\sigma_z\tau_x$ or $\delta H_4(\mathbf{k}) = f(\mathbf{k})\tau_y$ where

$$f(\mathbf{k}) = m'(\cos k_x - \cos k_y) \sin k_z. \quad (10)$$

As shown later in numerics, such a symmetry-allowed higher-order term in $k \cdot p$ theory can indeed change the structure of surface states on side surfaces.

In Fig. 1(b,c) we schematically depict possible evolutions of surface double Fermi arcs in the presence of symmetry-allowed perturbations. These symmetric perturbations (e.g. adding perturbation $\delta H_4(\mathbf{k})$ to “ideal Hamiltonian” (1)) are inevitable in real materials, and they will deform the double Fermi arcs to a closed contour enclosing the surface BZ center. Such a closed Fermi pocket can further shrink into a point on side surfaces.

C. Numerical results

Numerical results of spectral density $A(\mathbf{k}, \omega) = -\frac{1}{\pi} \text{Im}G(\mathbf{k}, \omega)$ assuming the Fermi energy lines up with bulk nodes are shown in Fig. 2. Here $G(\mathbf{k}, \omega)$ represents the electron Green function. We consider a slab geometry which is open along \hat{x} -direction and translational invariant in \hat{y} - \hat{z} plane. Therefore the surface and bulk spectral density are shown as a function of in-plane momentum $\mathbf{k}_{//} = (k_y, k_z)$.

Fig. 2(a) shows the surface spectral density of the four-band model (1). Gapless surface states are concentrated around $k_y = 0$ but extended along the k_z axis between the projected bulk nodes. Here two Fermi arcs are straight lines sitting on each other. This is due to the fact that all operators in minimal model (1) anti-commute with each other leading to a symmetric spectrum w.r.t zero energy. Notice that the model in (1), when $\varepsilon_{\mathbf{k}} = 0$, has also chiral symmetry as the Hamilto-

nian anti-commutes with $\sigma_z\tau_x$ and τ_y . Adding a dispersive term that preserves all symmetries, such as

$$\varepsilon_{\mathbf{k}} = t_1(\cos k_z - \cos Q) + t_2(\cos k_x + \cos k_y - 2) \quad (11)$$

or $\varepsilon_{\mathbf{k}} = t_1(\cos k_z - \cos Q)(\cos k_x + \cos k_y)$ make the spectrum to become asymmetric and will provide curvature to the double Fermi arcs as shown in Fig. 2(d). Note that the term $\varepsilon_{\mathbf{k}}$ neither moves the location of Dirac nodes in 1st BZ nor shift them in energy, so the two Dirac nodes remain as the only gap-closing points in the bulk.

Now let's introduce fully-symmetric perturbation (10) to the system. Panels in Fig. 2(b) and Fig. 2(e) clearly show that this perturbation, chosen as $m' = 0.4t$, deforms the Fermi arcs into a closed Fermi pocket. Further enhancement of $m' = 0.8t$ shrink the arcs to even smaller pockets as shown in Fig. 2(c) and Fig. 2(f). Note that while double Fermi arcs are deformed and mostly removed on the surface, the bulk states near the Fermi energy are not affected by these perturbations as shown in Fig. 2(g)-(k).

Before closing this section we would like to put our results and arguments with recent experiment on (100) side surface of Na_3Bi ¹⁹, where the existence of Fermi arcs was reported. This finding doesn't contradict with our theory of not “topologically” protected Fermi arcs. The reason is that the additional perturbations $\delta H_4(\mathbf{k})$ with k -dependent expression given quoted in (10) are usually higher order terms. Considering the fact that the Dirac nodes observed in these materials are close to Γ , these terms are essentially small and their effect could be out of experimental resolution.

III. TOPOLOGICAL CLASSIFICATION OF SURFACE STATES IN CD_3AS_2 AND NA_3BI

The above numerical calculations based upon 4-band model (1) and associated symmetric perturbations $\delta H_4(\mathbf{k})$ provide strong evidence that double Fermi arcs are not stable against perturbations, and gapless surface states on side surfaces of Dirac semimetals are only robust in $k_z = 0$ plane. One natural question is: beyond the description of 4-band model, do our conclusions still hold in complicated real materials of Dirac semimetals? In this section, we shall provide a positive answer for recently discovered Dirac materials Na_3Bi ^{14,15,19} and Cd_3As_2 ¹⁶⁻¹⁸. In the mathematical framework of K-theory we classify the stability of surface states on different side surfaces. In this approach, our considerations only depend on their space group and time reversal symmetries and therefore are quite generic, directly applying to real materials and experiments.

A. Symmetry classification of Na_3Bi

The space group of Dirac semimetal Na_3Bi is centrosymmetric $\text{P6}_3/\text{mmc}$ (No. 194)¹². The space group

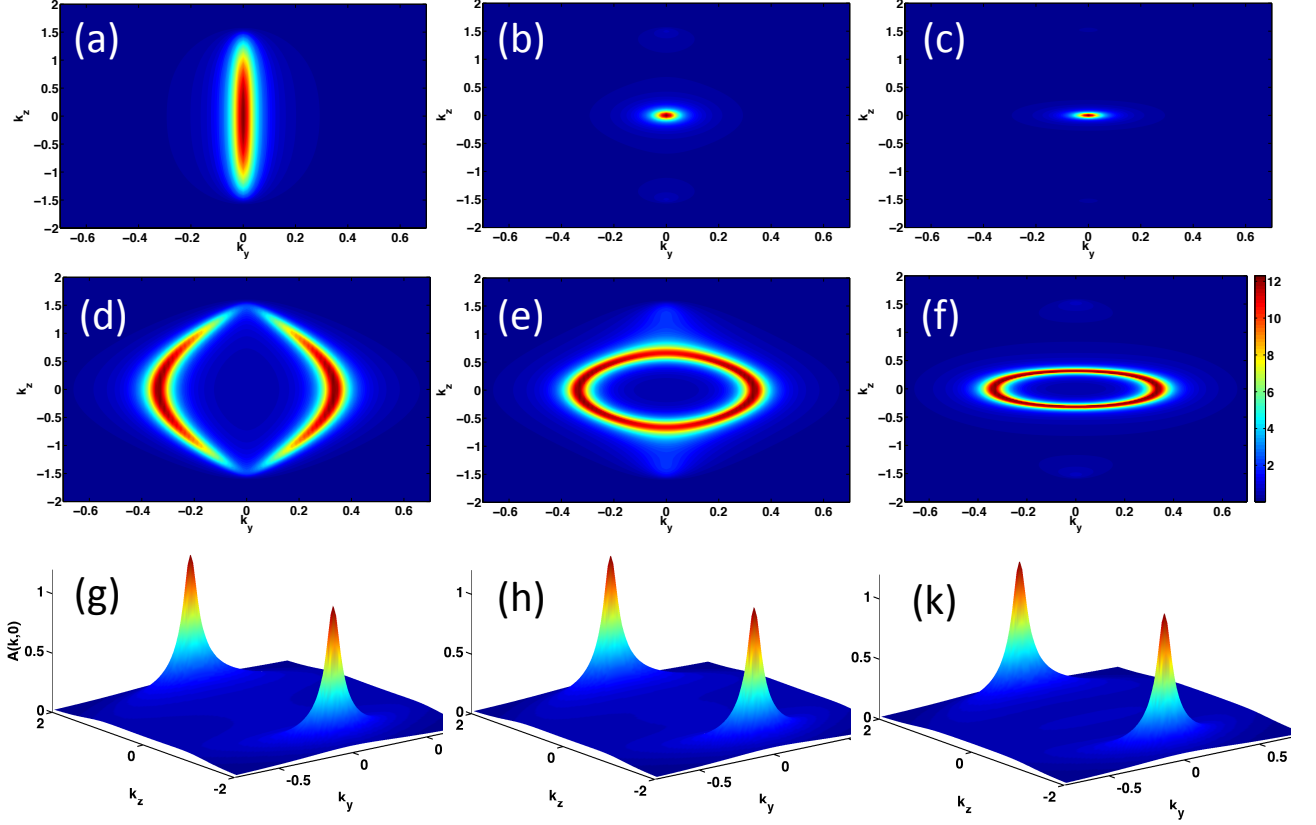


FIG. 2. (Color online) Spectral density of (a)-(f) the surface and (g)-(k) the bulk for a finite size system along x direction described by a four-band model in Eq. 1. Column-wise from left to right corresponds to adding a perturbation preserving all symmetries of the system with $m' = 0$, $m' = 0.4t$ and $m' = 0.8t$, respectively. In the absence of perturbation the surface states are either a line (a) or arcs (d) connecting projected bulk nodes. As soon as the perturbation is tuned on, the surface states start to disappear from the surface for both line (b)-(d) and arcs (e)-(f). In this process the bulk spectrum doesn't change as clearly seen from left to right in (g)-(k).

has 24 symmetry elements generated by 6-fold screw s_6 , glide reflection g_c and inversion I as follows.

$$(x, y, z) \xrightarrow{s_6} (x - y, x, z + 1/2), \quad (12)$$

$$(x, y, z) \xrightarrow{g_c} (y, x, z + 1/2), \quad (13)$$

$$(x, y, z) \xrightarrow{I} (-x, -y, -z), \quad (14)$$

which together with Bravais lattice translations $T_{a,b,c}$ generate all symmetry elements. Here the unit cell is expanded by $\mathbf{a} = a(1, 0, 0)$, $\mathbf{b} = a(-1/2, \sqrt{3}/2, 0)$ and $\mathbf{c} = c(0, 0, 1)$, and any real space point is represented as $\mathbf{r} = x\mathbf{a} + y\mathbf{b} + z\mathbf{c}$. The associated reciprocal lattice vectors are as $\mathbf{G}_a = 2\pi/a(1, 1/\sqrt{3}, 0)$, $\mathbf{G}_b = 2\pi/a(0, 2/\sqrt{3}, 0)$ and $\mathbf{G}_c = 2\pi/c(0, 0, 1)$.

The two Dirac nodes in bulk of Na_3Bi are located along c -axis at $\mathbf{Q}_\pm = \pm Q_0 \mathbf{G}_c$.¹² We are interested in side surfaces parallel to node separations which could host possible double Fermi arcs if stable at all. In following we show that there is no topological protection for the double Fermi arcs from lattice and time reversal symmetries.

1. Side surface (100)

The side surface (100) is parallel to \mathbf{a} and \mathbf{c} . Therefore, it remains invariant under following symmetries.

$$(x, y, z) \xrightarrow{R_b} (x, x - y, z), \quad R_b = T_c^{-1} g_c s_6 \quad (15)$$

$$(x, y, z) \xrightarrow{R_c} (x, y, 1/2 - z), \quad R_c = T_c^2 I s_6^3 \quad (16)$$

$$(x, y, z) \xrightarrow{C_2} (x, x - y, 1/2 - z), \quad C_2 = T_c^2 I s_6^2 g_c. \quad (17)$$

Note that $C_2 = T_c R_c R_b$. The following identities also hold

$$R_b^2 = R_c^2 = -1, \quad (18)$$

$$R_b R_c = -R_c R_b, \quad (19)$$

where the minus sign comes from 2π spin rotations associated with spatial rotations due to spin-orbit coupling.

In order to examine the effect of symmetries on Bloch Hamiltonian in momentum space, we introduce an or-

thogonal coordinates with unite vectors as follows.

$$\mathbf{k}_1 = (\sqrt{3}/2, 1/2, 0), \quad (20)$$

$$\mathbf{k}_2 = (-1/2, \sqrt{3}/2, 0), \quad (21)$$

$$\mathbf{k}_3 = (0, 0, 1). \quad (22)$$

Thus, any vector in Brillouin zone is represented as $\mathbf{k} = \sum_{i=1}^3 k_i \mathbf{k}_i$. Under crystalline symmetry operators above, we obtain

$$(k_1, k_2, k_3) \xrightarrow{R_b} (k_1, -k_2, k_3), \quad (23)$$

$$(k_1, k_2, k_3) \xrightarrow{R_c} (k_1, k_2, -k_3), \quad (24)$$

and under time reversal

$$(k_1, k_2, k_3) \xrightarrow{\Theta} (-k_1, -k_2, -k_3). \quad (25)$$

Assuming U_b and U_c correspond to representations of symmetry operations R_b and R_c acting on orbital and spin degrees of freedoms, the symmetric Bloch Hamiltonian transforms as

$$U_b H(k_1, k_2, k_3) U_b^{-1} = H(k_1, -k_2, k_3), \quad (26)$$

$$U_c H(k_1, k_2, k_3) U_c^{-1} = H(k_1, k_2, -k_3), \quad (27)$$

$$\Theta H(k_1, k_2, k_3) \Theta^{-1} = H(-k_1, -k_2, -k_3). \quad (28)$$

From these relations it is clear that symmetry operators U_b and $\Theta_c = \Theta U_c$ (a combination of time reversal Θ and reflection R_c) preserve a two-dimensional plane at fixed $k_3 \neq 0, \pi$ in momentum space, because

$$\Theta_c H(k_1, k_2, k_3) \Theta_c^{-1} = H(-k_1, -k_2, k_3). \quad (29)$$

Such two-dimensional planes are all gapped except for those passing through nodes at Q_{\pm} . Thus, we can classify gapped two-dimensional insulators embedded in the 3D Brillouin zone. Following the K-theory approach²⁸⁻³⁰, we classify gapped free-fermion quantum phases by examining the structure of *classifying space* for symmetry-allowed mass terms γ_0 in generic Dirac Hamiltonians:

$$H = k_1 \gamma_1 + k_2 \gamma_2 + m \gamma_0, \quad (30)$$

where γ_i 's satisfy Clifford algebra

$$\{\gamma_i, \gamma_j\} = \pm 2\delta_{ij}, \quad (31)$$

where $+$ ($-$) sign holds for $i, j = 1, 2(0)$. The symmetry operators satisfy that

$$U_b \gamma_1 U_b^{-1} = \gamma_1, \quad (32)$$

$$U_b \gamma_2 U_b^{-1} = -\gamma_2, \quad (33)$$

$$U_b \gamma_0 U_b^{-1} = \gamma_0, \quad (34)$$

$$\Theta_c \gamma_i \Theta_c^{-1} = -\gamma_i, \quad i = 0, 1, 2. \quad (35)$$

In addition to above symmetries, we also need to consider charge symmetry $U(1)_c$ generated by \mathbf{Q} , under which every fermion annihilation operator f is multiplied by the imaginary number: $f \xrightarrow{\mathbf{Q}} \imath f$. Therefore we have

$$\mathbf{Q}^2 = (U_b)^2 = -1, \quad (\Theta_c)^2 = +1, \quad (36)$$

$$\{\Theta_c, \mathbf{Q}\} = [U_b, \mathbf{Q}] = [\gamma_i, \mathbf{Q}] = 0, \quad (37)$$

$$\{U_b, U_c\} = [\Theta, U_{b,c}] = 0, \quad (38)$$

The whole 2D system therefore is characterized by symmetry generators $G = \{\Theta_c, U_b, \mathbf{Q}\}$, gamma matrices $\gamma_{1,2}$ and mass term γ_0 . Using these operators, we can construct a group of operators all anticommute with each other, which form the following *real Clifford algebra*

$$Cl_{5,0} = \{\gamma_1 \Theta_c, \gamma_2 \Theta_c, \mathbf{Q}, \gamma_1 U_b \Theta_c, \gamma_1 \gamma_2 \Theta_c \mathbf{Q}\}, \quad (39)$$

where all operators square -1 individually. The classification of 2D gapped phases amounts to the extension of this Clifford algebra by adding a mass term:

$$Cl_{5,0} \rightarrow Cl_{6,0} = \{\dots, \gamma_0 \gamma_1 \gamma_2 \Theta_c \mathbf{Q}\}. \quad (40)$$

since all term square as -1. The associated classifying space for mass term in such extension $Cl_{p,q} \rightarrow Cl_{p+1,q}$ is R_{p-q+2} , and the topological classification is given by zeroth homotopy of classifying space $\pi_0(R_{p-q+2})$. Thus we obtain

$$\pi_0(R_7) = 0 \quad (41)$$

implying that the classification is trivial and no protected surface states in a generic $k_z \neq 0, \pi$ plane on side surface (100).

The trivial classification implies that any counter propagating edge states on any fixed- k_z ($k_z \neq 0, \pi$) plane can be gapped out by symmetry-preserving perturbations. As mentioned in the previous section, the edge Hamiltonian takes a form $h = v_F \sum_k k \psi_k^\dagger \mu_z \psi_k$, where $\psi = (\psi_R, \psi_L)^T$. In this basis the symmetry operators are as $\Theta = \imath \mu_y \mathcal{K}$, $U_c = \imath \mu_z$ and $U_b = \imath \mu_y$. Therefore, a mass term like $m \mu_y$ preserving symmetries $\Theta_c = \imath \mu_x \mathcal{K}$ and U_b can be added to remove the surface states.

2. Side surface (110)

The side surface (110) is perpendicular to $\mathbf{G}_a + \mathbf{G}_b$ and hence parallel to Bravais vectors $\mathbf{a} - \mathbf{b}$ and \mathbf{c} . This plane breaks most crystalline symmetries except for those generated by glide g_c and reflection R_c acting on lattice sites as

$$(x, y, z) \xrightarrow{g_c} (y, x, z + 1/2), \quad (42)$$

$$(x, y, z) \xrightarrow{R_c} (x, y, 1/2 - z), \quad (43)$$

$$(x, y, z) \xrightarrow{C_2} (y, x, -z), \quad (44)$$

where $C_2 = R_c g_c$ and

$$(g_c)^2 = -T_c, \quad (45)$$

$$g_c R_c = -T_c R_c g_c. \quad (46)$$

As before, we introduce orthogonal coordinates with unite vector \mathbf{k}_1 perpendicular to (110) plane as follows.

$$\mathbf{k}_1 = (1/2, \sqrt{3}/2, 0), \quad (47)$$

$$\mathbf{k}_2 = (-\sqrt{3}/2, 1/2, 0), \quad (48)$$

$$\mathbf{k}_3 = (0, 0, 1). \quad (49)$$

Under crystalline symmetry operators above, we obtain

$$(k_1, k_2, k_3) \xrightarrow{g_c} (k_1, -k_2, k_3), \quad (50)$$

$$(k_1, k_2, k_3) \xrightarrow{R_c} (k_1, k_2, -k_3). \quad (51)$$

The symmetric Bloch Hamiltonian transforms as

$$U_g H(k_1, k_2, k_3) U_g^{-1} = H(k_1, -k_2, k_3), \quad (52)$$

$$U_c H(k_1, k_2, k_3) U_c^{-1} = H(k_1, k_2, -k_3), \quad (53)$$

$$\Theta H(k_1, k_2, k_3) \Theta^{-1} = H(-k_1, -k_2, -k_3), \quad (54)$$

where U_g implements glide g_c in spin and orbital basis.

Similar to the side surface (100), here for side surface (110) one can explicitly show that the edge states at fixed $k_z \neq 0, \pi$, if any, can be gapped out without breaking any symmetry on the surface. To show this, consider a pair of counter-propagating edge modes described by $h = v_F \sum_k k \psi_k^\dagger \mu_z \psi_k$ with symmetry operations represented as

$$\Theta_c = \Theta \cdot U_c = i\mu_y \mathcal{K} \cdot i\mu_z = i\mu_x \mathcal{K}, \quad (55)$$

$$U_g = i e^{ik_z/2} \mu_y. \quad (56)$$

A mass term like $\hat{M} = m \sum_k \psi_k^\dagger \gamma_0 \psi_k$ must satisfy

$$\{\mu_z, \gamma_0\} = [\Theta_c, \gamma_0] = [U_c, \gamma_0] = 0. \quad (57)$$

Clearly a symmetric mass term $\gamma_0 = \mu_y$ can destroy the edge states. Therefore there is no topological protection for surface states at $k_z \neq 0, \pi$ on side surface (110) either.

3. Surface states at $k_z = 0, \pi$

On both side surfaces (100) and (110) studied above, momentum cuts at $k_z = 0, \pi$ are special in the sense that the associated 2D system has more symmetries. In particular these momenta are TRI: i.e. their 2D Hamiltonians are invariant under mirror U_c and time reversal Θ symmetries separately.

With just time reversal $\Theta^2 = -1$ and charge conservation \mathbf{Q} , the corresponding real Clifford algebra and its extension are given as

$$Cl_{2,2} = \{\gamma_1, \gamma_2, \Theta, \Theta \mathbf{Q}\}, \quad (58)$$

$$Cl_{2,2} \rightarrow Cl_{3,2} = \{\dots, \gamma_0\}, \quad (59)$$

reproducing the well-known 2D index:

$$\pi_0(R_2) = \mathbb{Z}_2. \quad (60)$$

Remarkably, here nonsymmorphic glide reflection g_c with half translation along \hat{z} -axis provides extra constraints on these Z_2 indices. This nonsymmorphic glide forbids any nontrivial Z_2 index at $k_z = \pi$ plane³⁷, as will be shown below.

Let's consider crystal symmetries g_c, R_c as well in $k_z = 0, \pi$ planes with open (110) side surface. From (45)-(46) we know that $R_c^2 = -1$ and

$$(g_c)^2 = -1, \quad \{g_c, R_c\} = 0 \quad \text{at } k_z = 0; \quad (61)$$

while

$$(g_c)^2 = 1, \quad [g_c, R_c] = 0 \quad \text{at } k_z = \pi. \quad (62)$$

Therefore in $k_z = \pi$ plane, the associated *complex Clifford algebra* and extension problem are

$$Cl_5 = \{\gamma_1, \gamma_2, \Theta, \Theta \mathbf{Q}, g_c \gamma_2\} \times R_c, \quad (63)$$

$$Cl_5 \rightarrow Cl_6 = \{\dots, \gamma_0\}. \quad (64)$$

since R_c commutes with all other generators. This leads to a classifying space C_5 and trivial classification

$$\pi_0(C_5) = 0. \quad (65)$$

This proves the absence of any protected surface states at $k_z = \pi$ on side surface of Na_3Bi .

In $k_z = 0$ plane on the other hand, we found the Clifford algebra as follows

$$Cl_{4,2} = \{\gamma_1, \gamma_2, \Theta, \Theta \mathbf{Q}, g_c \gamma_2, R_c g_c \gamma_2\} \quad (66)$$

$$Cl_{4,2} \rightarrow Cl_{5,2} = \{\dots, \gamma_0\}. \quad (67)$$

The corresponding classifying space is $R_{2-4+2} = R_0$ leading to an integer classification

$$\pi_0(R_0) = \mathbb{Z}. \quad (68)$$

This integer index ν simply labels how many pairs of counter-propagating edge modes appear in $k_z = 0$ plane on side surface. In the case of Na_3Bi , both experiments and effective model (B4) indicates $\nu = 1$, i.e. $k_z = 0$ plane is a 2D topological insulator.

B. Symmetry classification of Cd_3As_2

The space group of Dirac semimetal Cd_3As_2 is centrosymmetric $I4_1/acd$ (No. 142).³⁹ In addition to Bravais lattice translations, it is generated by 4-fold screw rotation along \hat{z} -axis, glide reflection g_c and inversion I defined as follows.

$$(x, y, z) \xrightarrow{s_4} (y, 1/2 - x, 1/4 + z), \quad (69)$$

$$(x, y, z) \xrightarrow{g_c} (x, -y, 1/2 + z), \quad (70)$$

$$(x, y, z) \xrightarrow{I} (-x, 1/2 - y, 1/4 - z), \quad (71)$$

where $(s_4)^4 = (g_c)^2 = -T_z$. The Bravais lattice is expanded by $T_{\pm 1, \pm 1, \pm 1} \equiv (\pm 1, \pm 1, \pm 1)/2$ similar to BCC lattice. Two Dirac nodes in Cd_3As_2 is located along the \hat{z} -axis. There are two inequivalent side surfaces parallel to node separation, i.e. (100) and (110) surfaces. Completely similar to Na_3Bi case, here nonsymmorphic glide reflection g_c dictates that $k_z = \pi$ plane must have a trivial Z_2 index with no protected surface states on side surfaces, while $k_z = 0$ plane can support a nontrivial Z_2 QSH index. Indeed experiments and minimal models (1) suggest that $k_z = 0$ plane is a 2D insulator, leading to protected $k_z = 0$ surface states on side surfaces of Cd_3As_2 . In the following we analyze stability of generic surface states on two representative side surfaces.

1. Side surface (100)

This side surface preserves a symmetry subgroup generated by two glides

$$(x, y, z) \xrightarrow{g_c} (x, -y, 1/2 + z), \quad (72)$$

$$(x, y, z) \xrightarrow{g_b} (x, 1/2 + y, 1/4 - z), \quad (73)$$

where

$$g_b = T_{\bar{1}\bar{1}\bar{1}} I(s_4)^2 \Rightarrow (g_b)^2 = -T_y, \quad (74)$$

$$g_b g_c = -T_y T_z^{-1} g_c g_b. \quad (75)$$

In an orthogonal basis the Bloch Hamiltonian transforms as

$$U_{g_c} H(k_x, k_y, k_z) U_{g_c}^{-1} = H(k_x, -k_y, k_z), \quad (76)$$

$$U_{g_b} H(k_x, k_y, k_z) U_{g_b}^{-1} = H(k_x, k_y, -k_z). \quad (77)$$

We define

$$\Theta_{g_b} = \Theta U_{g_b}, \quad (78)$$

which transform the Bloch Hamiltonian as

$$\Theta_{g_b} H(k_x, k_y, k_z) \Theta_{g_b}^{-1} = H(-k_x, -k_y, k_z). \quad (79)$$

In momentum space we have

$$U_{g_c}^2 = -e^{ik_z}, \quad (80)$$

$$\Theta_{g_b}^2 = e^{ik_y}, \quad (81)$$

$$\Theta_{g_b} U_{g_c} \Theta_{g_b}^{-1} = -e^{i(k_y - k_z)} U_{g_c}. \quad (82)$$

As before we focus on planes with fixed $k_z \neq 0, \pi$. At $k_y = 0, \pi$ the effective time reversal symmetry squares $\Theta_{g_b}^2 = \pm 1$, which leads to a one dimensional classification for Hamiltonian:

$$H(k_x) = k_x \gamma_x + m \gamma_0. \quad (83)$$

At $k_y = 0$, the corresponding Clifford algebras and its extension become as follows.

$$Cl_{0,3} = \{\gamma_x, \Theta_{g_b}, \Theta_{g_b} \mathbf{Q}\}, \quad (84)$$

$$Cl_{0,3} \rightarrow Cl_{1,3} = \{\dots, \gamma_0\}. \quad (85)$$

As a result the classification is given by

$$\pi_0(R_{0-3+2}) = 0. \quad (86)$$

At $k_y = \pi$, the corresponding Clifford algebras and its extension remain the same as above, and since $\Theta_{g_b}^2 = -1$ at $k_y = \pi$ the classification to be trivial as follows

$$\pi_0(R_{2-1+2}) = 0. \quad (87)$$

One can also understand the robustness of surface states in terms of low-energy effective Hamiltonian. Consider a pair of counter-propagating edge modes at fixed $k_z \neq 0, \pi$, described by $h(k_y) = v_F k_y \mu_z$. In following we show that a mass term δh is allowed by symmetry

to gap out these surface states at $k_z \neq 0, \pi$. The transformation of mass term is given as follows. A minimal representation of symmetry operators is as follows.

$$U_{g_c}(\mathbf{k}) = i\mu_y e^{ik_z/2}, \quad (88)$$

$$\Theta_{g_b}(\mathbf{k}) = i\mu_x e^{ik_y/2} \mathcal{K}. \quad (89)$$

The symmetric mass term is found to be $\delta h = m\mu_y$, which can destroy gapless surface states at fixed $k_z \neq 0, \pi$ on side surface (100).

2. Side surface (110)

There are two glides

$$(x, y, z) \xrightarrow{g_d} (y + 1/2, x, z + 1/4), \quad g_d = T_{\bar{1}\bar{1}\bar{1}} g_c s_4,$$

$$(x, y, z) \xrightarrow{g_b} (x, y + 1/2, 1/4 - z), \quad g_b = T_{\bar{1}\bar{1}\bar{1}} I(s_4)^2.$$

satisfying

$$(g_d)^2 = -T_{111}, \quad (g_b)^2 = -T_y,$$

$$g_b g_d g_b^{-1} = -T_{\bar{1}\bar{1}\bar{1}} g_d.$$

Although both glides are broken on side surface (110), there is a 2-fold rotation, the combination of two glides, preserved on (110) surface:

$$(x, y, z) \xrightarrow{C_2} (y, x, 1/2 - z), \quad C_2 = T_x^{-1} g_d g_b.$$

The combination Θ_{C_2} of time reversal Θ and C_2 rotation satisfying $(\Theta_{C_2})^2 = 1$ preserves each surface momenta, but the classification of 1d system at fixed $k_x - k_y$ and k_z is trivial

$$\pi_0(R_{0-3+2}) = 0 \quad (90)$$

from Clifford algebra and extension problem

$$Cl_{0,3} = \{\gamma_1, \Theta_{C_2}, \Theta_{C_2} \mathbf{Q}\}, \quad (91)$$

$$Cl_{0,3} \rightarrow Cl_{1,3} = \{\dots, \gamma_0\}. \quad (92)$$

$$(93)$$

Therefore generally surface states at $k_z \neq 0, \pi$ are not robust against perturbations on side surface (110).

IV. CONCLUSIONS

In this paper we study the topological stability of double Fermi arcs on side surfaces of Dirac semimetals. Using K-theory and symmetry analysis on the space groups of Dirac semimetal materials Cd_3As_3 and Na_3Bi , we show that most of the double Fermi arcs can be destroyed by symmetric perturbations without any symmetry breaking or bulk phase transitions, except for at $k_z = 0$ due to a nontrivial Z_2 index (see FIG. 1). This conclusion is further supported by numerical results of surface and bulk spectral functions in a slab geometry (see FIG. 2) based upon a symmetric minimal 4-band model^{12,13} for Dirac semimetals, which clearly shows that the double fermi arcs can be continuously deformed into a closed fermi pocket and eventually to a point at the surface BZ center.

ACKNOWLEDGMENTS

MK and MR acknowledge the support of the CEM, an NSF MRSEC, under grant DMR-1420451. YML thanks Aspen center for physics where part of the manuscript was written. YML acknowledges the startup funds at the Ohio State University and National Science Foundation grant PHY-1066293.

Appendix A: Equivalence between 4-band model (1) and effective $k \cdot p$ Hamiltonian for Cd_3As_2 and Na_3Bi

In this section we show that in the long-wavelength limit, the 4-band model (1) can be related to the following effective Hamiltonian derived from $k \cdot p$ theory^{40,41} around Γ point:

$$\hat{H}_\Gamma(\mathbf{k}) = \epsilon_{\mathbf{k}} + \begin{pmatrix} M(\mathbf{k}) & \lambda k_+ & 0 & 0 \\ \lambda k_- & -M(\mathbf{k}) & 0 & 0 \\ 0 & 0 & M(\mathbf{k}) & -\lambda k_- \\ 0 & 0 & -\lambda k_+ & -M(\mathbf{k}) \end{pmatrix} + O(|\mathbf{k}|^2), \quad (\text{A1})$$

which is widely adopted to describe topological properties of Dirac semimetal materials Na_3Bi ¹² and Cd_3As_2 ¹³. This effective $k \cdot p$ model is written in the basis of $|S_{J=\frac{1}{2}}, J_z = \frac{1}{2}\rangle, |P_{J=\frac{3}{2}}, J_z = \frac{3}{2}\rangle, |S_{J=\frac{1}{2}}, J_z = -\frac{1}{2}\rangle, |P_{J=\frac{3}{2}}, J_z = -\frac{3}{2}\rangle$. Using Pauli matrices $\vec{\sigma}$ for $J_z = \pm J$ index and $\vec{\tau}$ for total angular momentum J index, the above effective model can be written as

$$\hat{H}_\Gamma(\mathbf{k}) = \epsilon_{\mathbf{k}} + A(k_x \sigma_z \tau_x - k_y \sigma_0 \tau_y) + M(\mathbf{k}) \sigma_0 \tau_z + O(|\mathbf{k}|^2) \quad (\text{A2})$$

where $M(\mathbf{k}) = M_0 - M_1 k_z^2 - M_2(k_x^2 + k_y^2) + O(|\mathbf{k}|^2)$ with $M_0, M_1, M_2 < 0$. Under the unitary rotation

$$\hat{U} = i(\sin \varphi \sigma_x + \cos \varphi \sigma_y) \frac{1+\tau_z}{2} + e^{i\varphi \sigma_z} \frac{1-\tau_z}{2} \quad (\text{A3})$$

we obtain

$$\begin{aligned} H_4(\mathbf{k}) &= \hat{U}^\dagger \hat{H}_\Gamma(\mathbf{k}) \hat{U} \\ &= \lambda(k_x \sigma_x + k_y \sigma_y) \tau_x + M(\mathbf{k}) \sigma_0 \tau_z, \\ M(\mathbf{k}) &= t_z(1 - \cos Q) - \frac{t_z}{2} k_z^2 - \frac{t}{2}(k_x^2 + k_y^2) + O(|\mathbf{k}|^2). \end{aligned}$$

Therefore unitary rotation (A3) indeed transforms effective $k \cdot p$ Hamiltonian (A2) which describes Dirac semimetal materials into the 4-band minimal model (1) used for calculations in this paper.

The symmetry operations $\psi_{\mathbf{k}}$ for $k \cdot p$ model (A2) are summarized as follows:

$$\hat{T} = i\sigma_y \cdot \mathcal{K}; \quad (\text{A4})$$

$$\hat{s}_n = e^{i\frac{\pi}{n}\sigma_z(2-\tau_z)}, \quad n = 4, 6; \quad (\text{A5})$$

$$\hat{I} = \tau_z, \quad (x, y, z) \rightarrow (-x, -y, -z); \quad (\text{A6})$$

$$\hat{g}_c = i\sigma_x : \quad (x, y, z) \rightarrow (-x, y, z + \frac{1}{2}). \quad (\text{A7})$$

After the unitary rotation (A3) we can obtain the symmetry operations for 4-band model (1):

$$\tilde{T} = i\sigma_y \cdot \mathcal{K}; \quad (\text{A8})$$

$$\tilde{s}_n = e^{i\frac{\pi}{n}\sigma_z(1-2\tau_z)}, \quad n = 4, 6; \quad (\text{A9})$$

$$\tilde{I} = \tau_z : \quad (x, y, z) \rightarrow (-x, -y, -z); \quad (\text{A10})$$

$$\tilde{g}_c = i\sigma_x \tau_z : \quad (x, y, z) \rightarrow (-x, y, z + \frac{1}{2}). \quad (\text{A11})$$

where we've chose $\varphi = 0$ for simplicity in unitary rotation (A3). For the purpose of simplicity, in most discussions we will simply treat the nonsymmorphic n -fold screw rotation s_n as a symmorphic n -fold rotation C_n^z , and the glide symmetry g_c as a symmorphic mirror reflection symmetry R_x .

Appendix B: 4-band Tight-binding Model for Dirac semimetal Na_3Bi

With $n = 6$ -fold rotational symmetry along \hat{z} -axis, Na_3Bi has a hexagonal Brillouin zone in $\hat{x} - \hat{y}$ plane. Choosing $\vec{a}_1 = (1, 0)$ and $\vec{a}_2 = (1, \sqrt{3})/2$ as the Bravais lattice unit vectors, the primitive vectors of reciprocal lattice in $\hat{x} - \hat{y}$ plane are $\vec{b}_1 = (\sqrt{3}, -1)/\sqrt{3}$ and $\vec{b}_2 = (0, 2)/\sqrt{3}$. The momentum space is hence parametrized as

$$\mathbf{k} = (k_x, k_y, k_z) = (k_1, \frac{2k_2 - k_1}{\sqrt{3}}, k_3). \quad (\text{B1})$$

where under 6-fold rotation $C_6^z = e^{i\pi\sigma_z(1-2\tau_z)/6}$ we have

$$(k_1, k_2, k_3) \xrightarrow{C_6^z} (k_1 - k_2, -k_1, k_3). \quad (\text{B2})$$

and under mirror reflection $R_x = i\sigma_x \tau_z$

$$(k_1, k_2, k_3) \xrightarrow{R_x} (-k_1, k_2 - k_1, k_3). \quad (\text{B3})$$

As a result, the 4-band minimal tight-binding model describing Dirac semimetal Na_3Bi is

$$\begin{aligned} H_4(\mathbf{k}) &= \lambda \left[\sigma_x \sin k_1 + \frac{\sigma_x - \sqrt{3}\sigma_y}{2} \sin(k_1 - k_2) \right. \\ &\quad \left. + \frac{\sigma_x + \sqrt{3}\sigma_y}{2} \sin k_2 \right] \tau_x \\ &\quad + \left[t(\cos k_1 + \cos k_2 + \cos(k_1 - k_2) - 3) \right. \\ &\quad \left. + t_z(\cos k_z - \cos Q) \right] \tau_z. \end{aligned} \quad (\text{B4})$$

Clearly it preserves time reversal and all space group symmetries, the same as Cd_3As_2 case (1).

Similar to Cd_3As_2 case with 4-fold rotations, Na_3Bi with 6-fold rotation axis allow the following symmetric perturbations to minimal model $H_4(\mathbf{k})$:

$$\begin{aligned} \delta H_4(\mathbf{k}) &= \Delta \sin k_z \left[\sigma_z \tau_x \cos k_1 + \frac{-\sigma_z \tau_x + \sqrt{3}\tau_y}{2} \cos(k_1 - k_2) \right. \\ &\quad \left. - \frac{\sigma_z \tau_x + \sqrt{3}\tau_y}{2} \cos k_2 \right] \end{aligned} \quad (\text{B5})$$

just like (10) in Cd_3As_2 case. This symmetric term can continuously deform the double Fermi-arc on the side surface into a closed pocket.

- ¹ M. Z. Hasan and C. L. Kane, *Rev. Mod. Phys.*, **82**, 3045 (2010).
- ² X.-L. Qi and S.-C. Zhang, *Rev. Mod. Phys.*, **83**, 1057 (2011).
- ³ M. Z. Hasan and J. E. Moore, *Annual Review of Condensed Matter Physics*, **2**, 55 (2011).
- ⁴ G. E. Volovik, *The Universe in a Helium Droplet* (Clarendon Press, Oxford, England, 2003).
- ⁵ P. Horava, *Phys. Rev. Lett.*, **95**, 016405 (2005).
- ⁶ X. Wan, A. M. Turner, A. Vishwanath, and S. Y. Savrasov, *Phys. Rev. B*, **83**, 205101 (2011).
- ⁷ A. A. Burkov, M. D. Hook, and L. Balents, *Phys. Rev. B*, **84**, 235126 (2011).
- ⁸ Y. X. Zhao and Z. D. Wang, *Phys. Rev. Lett.*, **110**, 240404 (2013).
- ⁹ S. Matsuura, P.-Y. Chang, A. P. Schnyder, and S. Ryu, *New Journal of Physics*, **15**, 065001 (2013), ISSN 1367-2630.
- ¹⁰ O. Vafek and A. Vishwanath, *Annual Review of Condensed Matter Physics*, **5**, 83 (2014).
- ¹¹ S. M. Young, S. Zaheer, J. C. Y. Teo, C. L. Kane, E. J. Mele, and A. M. Rappe, *Phys. Rev. Lett.*, **108**, 140405 (2012).
- ¹² Z. Wang, Y. Sun, X.-Q. Chen, C. Franchini, G. Xu, H. Weng, X. Dai, and Z. Fang, *Phys. Rev. B*, **85**, 195320 (2012).
- ¹³ Z. Wang, H. Weng, Q. Wu, X. Dai, and Z. Fang, *Phys. Rev. B*, **88**, 125427 (2013).
- ¹⁴ Z. K. Liu, B. Zhou, Y. Zhang, Z. J. Wang, H. M. Weng, D. Prabhakaran, S.-K. Mo, Z. X. Shen, Z. Fang, X. Dai, Z. Hussain, and Y. L. Chen, *Science*, **343**, 864 (2014).
- ¹⁵ J. Xiong, S. Kushwaha, J. Krizan, T. Liang, R. J. Cava, and N. P. Ong, arXiv:1502.06266.
- ¹⁶ H. Yi, Z. Wang, C. Chen, Y. Shi, Y. Feng, A. Liang, Z. Xie, S. He, J. He, Y. Peng, X. Liu, Y. Liu, L. Zhao, G. Liu, X. Dong, J. Zhang, M. Nakatake, M. Arita, K. Shimada, H. Namatame, M. Taniguchi, Z. Xu, C. Chen, X. Dai, Z. Fang, and X. J. Zhou, *Sci. Rep.*, **4** (2014).
- ¹⁷ M. Neupane, S.-Y. Xu, R. Sankar, N. Alidoust, G. Bian, C. Liu, I. Belopolski, T.-R. Chang, H.-T. Jeng, H. Lin, A. Bansil, F. Chou, and M. Z. Hasan, *Nat Commun*, **5** (2014).
- ¹⁸ S. Jeon, B. B. Zhou, A. Gyenis, B. E. Feldman, I. Kimchi, A. C. Potter, Q. D. Gibson, R. J. Cava, A. Vishwanath, and A. Yazdani, *Nat Mater*, **13**, 851 (2014).
- ¹⁹ S.-Y. Xu, C. Liu, S. K. Kushwaha, R. Sankar, J. W. Krizan, I. Belopolski, M. Neupane, G. Bian, N. Alidoust, T.-R. Chang, H.-T. Jeng, C.-Y. Huang, W.-F. Tsai, H. Lin, P. P. Shibayev, F.-C. Chou, R. J. Cava, and M. Z. Hasan, *Science*, **347**, 294 (2015).
- ²⁰ P. J. Moll, L. N. Nair, T. Helm, A. C. Potter, I. Kimchi, A. Vishwanath, and J. G. Analytis, arXiv:1505.02817 (2015).
- ²¹ B.-J. Yang and N. Nagaosa, *Phys. Rev. Lett.*, **112**, 246402 (2014).
- ²² S.-Y. Xu, I. Belopolski, N. Alidoust, M. Neupane, C. Zhang, R. Sankar, S.-M. Huang, C.-C. Lee, G. Chang, B. Wang, G. Bian, H. Zheng, D. S. Sancez, A. Bansil, F. Chou, H. Lin, S. Jia, and M. Z. Hasan, arXiv:1502.03807.
- ²³ H. Weng, C. Fang, Z. Fang, B. A. Bernevig, and X. Dai, *Phys. Rev. X*, **5**, 011029 (2015).
- ²⁴ B. Q. Lv, H. M. Weng, B. B. Fu, X. P. Wang, H. Miao, J. Ma, P. Richard, X. C. Huang, L. X. Zhao, G. F. Chen, Z. Fang, X. Dai, T. Qian, and H. Ding, *Phys. Rev. X*, **5**, 031013 (2015).
- ²⁵ B. Q. Lv, N. Xu, H. M. Weng, J. Z. Ma, P. Richard, X. C. Huang, L. X. Zhao, G. F. Chen, C. E. Matt, F. Bisti, V. N. Strocov, J. Mesot, Z. Fang, X. Dai, T. Qian, M. Shi, and H. Ding, *Nat Phys*, **11**, 724 (2015).
- ²⁶ A. C. Potter, I. Kimchi, and A. Vishwanath, *Nat Commun*, **5**, (2014).
- ²⁷ K.-Y. Yang, Y.-M. Lu, and Y. Ran, *Phys. Rev. B*, **84**, 075129 (2011).
- ²⁸ A. Kitaev, *AIP Conference Proceedings*, **1134**, 22 (2009).
- ²⁹ X.-G. Wen, *Phys. Rev. B*, **85**, 085103 (2012).
- ³⁰ T. Morimoto and A. Furusaki, *Phys. Rev. B*, **88**, 125129 (2013).
- ³¹ K. Shiozaki and M. Sato, *Phys. Rev. B*, **90**, 165114 (2014).
- ³² C.-K. Chiu and A. P. Schnyder, *Journal of Physics: Conference Series*, **603**, 012002 (2015).
- ³³ C. L. Kane and E. J. Mele, *Phys. Rev. Lett.*, **95**, 146802 (2005).
- ³⁴ C. L. Kane and E. J. Mele, *Phys. Rev. Lett.*, **95**, 226801 (2005).
- ³⁵ B. A. Bernevig, T. L. Hughes, and S.-C. Zhang, *Science*, **314**, 1757 (2006).
- ³⁶ M. König, S. Wiedmann, C. Brune, A. Roth, H. Buhmann, L. W. Molenkamp, X.-L. Qi, and S.-C. Zhang, *Science*, **318**, 766 (2007).
- ³⁷ D. Varjas, F. d. Juan, and Y.-M. Lu, to appear (see also <http://online.kitp.ucsb.edu/online/lsmatter-c15/lu/>).
- ³⁸ L. Fu and C. L. Kane, *Phys. Rev. B*, **74**, 195312 (2006).
- ³⁹ M. N. Ali, Q. Gibson, S. Jeon, B. B. Zhou, A. Yazdani, and R. J. Cava, *Inorganic Chemistry*, **53**, 4062 (2014).
- ⁴⁰ L. C. L. Y. Voon and M. Willatzen, *The $k \cdot p$ Method: Electronic Properties of Semiconductors* (Springer, 2009).
- ⁴¹ P. Yu and M. Cardona, *Fundamentals of Semiconductors: Physics and Materials Properties*, 4th ed., Graduate Texts in Physics (Springer, 2010).